Title

Prediction of mass and momentum transport in turbulent plane wall jets over smooth and transitionally rough surfaces

Journal

Environmental Fluid Mechanics, 16(3)

ISSN

1567-7419

Authors

Younis, BA
Zumdick, M
Weigand, B

Publication Date

2016-06-01

DOI

10.1007/s10652-015-9431-2

Peer reviewed

Environ Fluid Mech (2016) 16:485–502
DOI 10.1007/s10652-015-9431-2

ORIGINAL ARTICLE

Prediction of mass and momentum transport in turbulent plane wall jets over smooth and transitionally rough surfaces

B. A. Younis[1] · M. Zumdick[2] · B. Weigand[2]

Received: 30 April 2015 / Accepted: 10 October 2015 / Published online: 17 October 2015

Abstract This paper is concerned with the prediction of mass and momentum transport in turbulent wall jets developing over smooth and transitionally rough plane walls. The ability to accurately predict the resulting wall shear stresses and vertical profiles of the Reynolds stresses in these flows is prerequisite to the accurate prediction of bed scour, sediment re-suspension and transport by turbulent diffusion. The computations were performed by solving the Reynolds-averaged forms of the equations describing conservation of mass, momentum and concentration. The unknown correlations that arise from the averaging process (the Reynolds stresses in the case of the momentum equation, and the turbulent mass fluxes in the case of concentration) were obtained from the solution of modeled differential equations that describe their conservation. Since these models are somewhat more complex than those typically used in practice, their benefits are demonstrated by comparisons with results obtained from simpler, eddy-viscosity based closures. Comparisons with experimental data show that results of acceptable accuracy can be obtained only by using the appropriate combination of models for the turbulent fluxes of mass and momentum that properly account for the reduction of the Reynolds stresses due to wall damping effects, and for the modification of the mass transfer rates due to interactions with the mean rates of strain.

Keywords Turbulent wall jet · Transitional roughness · Turbulent mass transport

1 Introduction

The paper deals with the prediction of turbulent mass and momentum transport in jets developing over plane smooth and transitionally rough surfaces. Figure 1 shows a schematic of the flows considered, and defines various flow parameters. Turbulent wall jets are

✉ B. A. Younis
bayounis@ucdavis.edu

[1] Department of Civil & Environmental Engineering, University of California, Davis, CA, USA

[2] Institut für Thermodynamik der Luft- und Raumfahrt, Universität Stuttgart, Stuttgart, Germany

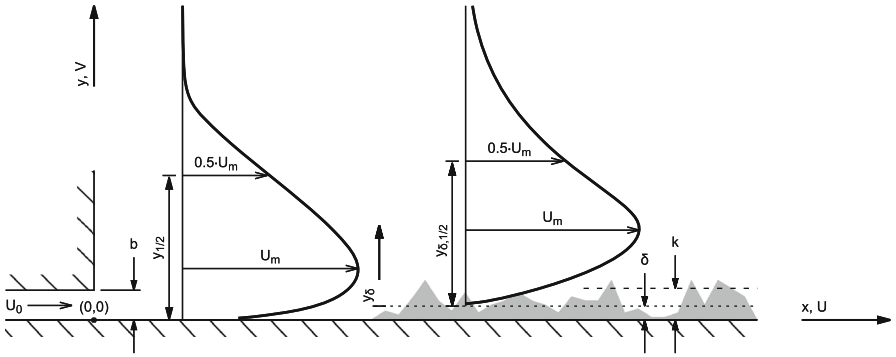

Fig. 1 Schematic of smooth and rough wall jets and their bulk parameters

encountered in nature in the form of gravity currents, avalanches and other large-scale suspension clouds Rastello and Hopfinger [1], Etienne et al. [2]. They also arise as turbidity current which are submerged sediment-laden flows that transport large volumes of sediment downslope in lakes and marine basins Kneller and Buckee [3], Gray et al. [4]. Their occurrence on erodible surfaces of cohesive or noncohesive materials is known to be the cause of significant local scour Mazurek et al. [5], Rajaratnam [6] and Hogg et al. [7]. The ability to accurately predict the turbulence field in a developing wall jet, and the associated mass transport, is essential to the accurate prediction of the evolution of scour holes, sediment suspension, and subsequent transport by the mean flow and turbulent diffusion. The prediction of the evolution of turbulent wall jets is not straightforward. The flow can be viewed as the combination of an outer free shear layer and a flat-plate boundary layer below it, divided by a mixing layer Barenblatt et al. [8]. Interactions occur across the interface (defined by the loci of points of maximum velocity) and extend deep within each layer. The intensity of these interactions increases with the difference between the jet's maximum velocity and that of the free stream and reaches a maximum when the jet develops in stagnant surroundings. Among the interesting consequence of this interaction is the separation between the points where the mean shear ($\partial U/\partial y$ in the notation of Fig. 1) and the shear stress are zero. The extent of this separation increases with streamwise development [9]. Boussinesq's assumption of a linear relationship between the turbulent stresses and the local mean rates of strain, the cornerstone of most practical turbulence closures, implies that these two points are always coincident. Clearly models which utilize this assumption will fail to correctly capture the consequences of this interaction on the transport processes that occur across the interface. The most notable of these is the significant reduction of the Reynolds stresses in the wall jet relative to an equivalent plane free jet Albayrak et al. [10]. Since most models for suspended sediment transport obtain the turbulent mass fluxes from Fick's law which is formulated by analogy to Boussinesq, then these models too are unlikely to yield the correct vertical profiles of suspended sediment. The limitations in Boussinesq do not arise in Reynolds-stress transport closures where the components of the Reynolds stress tensor are obtained from the solution of modeled differential transport equations describing their conservation. The same is true for the turbulent mass fluxes where obtaining them from the solution of their differential conservation equations obviates the need to rely on Fick's law. The primary objective of this paper is to determine whether adoption of these more complex turbulence closures leads to distinct improvements in the accuracy to which the Reynolds stresses and the turbulent mass fluxes can be predicted relative to the simpler gradient-transport closures.

2 The mathematical models

2.1 Mean-flow equations

The time-averaged equations for steady, constant property flow at high Reynolds number are written in Cartesian-tensor notation as follows:

$$\frac{\partial U_i}{\partial x_i} = 0 \tag{1}$$

$$U_j \frac{\partial U_i}{\partial x_j} = \frac{\partial}{\partial x_j}\left(\nu \frac{\partial U_i}{\partial x_j} - \overline{u_i u_j}\right) - \frac{1}{\rho}\frac{\partial p}{\partial x_i} \tag{2}$$

$$U_j \frac{\partial \Theta}{\partial x_j} = \frac{\partial}{\partial x_i}\left(\frac{\nu}{Sc_l}\frac{\partial \Theta}{\partial x_i} - \overline{u_i \theta}\right) \tag{3}$$

where Θ is a general transported scalar which in this study would be the concentration, ν is the kinematic viscosity, Sc is the molecular Schmidt number, and $\overline{u_i u_j}$ and $\overline{u_i \theta}$ are, respectively, the unknown Reynolds stresses and the turbulent mass fluxes.

2.2 The models for $\overline{u_i u_j}$

The eddy-viscosity closure used in this study utilizes Boussinesq's hypothesis which, as previously mentioned, makes the unknown turbulent stresses linearly proportional to the local mean rates of strain:

$$-\overline{u_i u_j} = \nu_t \left(\frac{\partial U_i}{\partial x_j} + \frac{\partial U_j}{\partial x_i}\right) - \frac{2}{3}\delta_{ij} k \tag{4}$$

where ν_t is the turbulent viscosity which in the present study is determined by using the k-ϵ model which is agruably the most widely turbulence closure in practice. In this model, ν_t is obtained from:

$$\nu_t = C_\mu \frac{k^2}{\epsilon} \tag{5}$$

where $C_\mu = 0.09$ and k and ϵ, respectively the turbulence kinetic energy and its dissipation rate, are obtained from the solution of the equations:

$$U_i \frac{\partial k}{\partial x_i} = \frac{\partial}{\partial x_i}\left(\frac{\nu_t}{\sigma_k}\frac{\partial k}{\partial x_i}\right) + P_k - \epsilon \tag{6}$$

$$U_i \frac{\partial \epsilon}{\partial x_i} = \frac{\partial}{\partial x_i}\left(\frac{\nu_t}{\sigma_\epsilon}\frac{\partial \epsilon}{\partial x_i}\right) + C_{\epsilon_1}\frac{\epsilon}{k}P_k - C_{\epsilon_2}\frac{\epsilon^2}{k} \tag{7}$$

where P_k is the rate of production of turbulence kinetic energy:

$$P_k = -\overline{u_i u_j}\left(\frac{\partial U_i}{\partial x_j} + \frac{\partial U_j}{\partial x_i}\right), \tag{8}$$

and the Cs and σs are coefficients assigned here their standard values: (C_{ϵ_1}, C_{ϵ_2}, σ_k, σ_ϵ) = (1.44, 1.92, 1.0, 1.22).

It is worth noting that substitution for $-\overline{u_i u_j}$ from Boussinesq in the expression for P_k precludes the latter from ever assuming negative values. For the case of a wall jet, and to the boundary-layer approximation of $\partial U/\partial y \gg \partial V/\partial x$, P_k does indeed become negative in the region in between the points where the locations where the shear stress is zero and the velocity is a maximum.

In Reynolds-stress transport closures, the Reynolds stresses are obtained from the following transport equation:

$$\overbrace{U_k \frac{\partial \overline{u_i u_j}}{\partial x_k}}^{\text{Convection: } C_{ij}} = \overbrace{-\left(\overline{u_i u_k}\frac{\partial U_j}{\partial x_k} + \overline{u_j u_k}\frac{\partial U_i}{\partial x_k}\right)}^{\text{Production: } P_{ij}} \overbrace{-\frac{\partial}{\partial x_k}\left[\overline{u_i u_j u_k} + \frac{1}{\rho}\left(\overline{p' u_i}\delta_{jk} + \overline{p' u_j}\delta_{ik}\right) - \nu\frac{\partial \overline{u_i u_j}}{\partial x_k}\right]}^{\text{Diffusion: } D_{ij}} \overbrace{-2\nu\left(\frac{\partial u_i}{\partial x_k}\frac{\partial u_j}{\partial x_k}\right)}^{\text{Dissipation: } \epsilon_{ij}} + \overbrace{\frac{p'}{\rho}\left(\frac{\partial u_i}{\partial x_j} + \frac{\partial u_j}{\partial x_i}\right)}^{\text{Redistribution: } \Phi_{ij}} \tag{9}$$

In the above, P_{ij}, the rate of production term which is exact and in no need of modeling. The diffusion term consists of three terms, namely turbulence fluctuations, pressure fluctuations and molecular diffusion of which only the latter is exact. In this work, the pressure diffusion term is neglected since the measurements of Irwin [11] in a turbulent wall jet show that it makes negligible contribution to the stress balances. The turbulent diffusion term is modeled as proposed by Daly and Harlow [12] i.e. by assuming that the diffusion of a component of the Reynolds stress tensor is proportional to its spatial gradient:

$$-\overline{u_i u_j u_k} = C_s \frac{k}{\epsilon}\overline{u_k u_l}\frac{\partial \overline{u_i u_j}}{\partial x_l} \tag{10}$$

The coefficient C_s is assigned its usual value of 0.22.

The physical role of the pressure-strain correlations term (Φ_{ij}) is to redistribute the turbulence energy amongst the three normal-stress components and to reduce the shear stresses. It is therefore the most direct agency through which the damping effects of a solid wall are felt within both the wall and the free shear layers and is thus expected to play a major role in the prediction of wall jets. The literature contains several proposals for modeling this term most of which can be expressed in a unified form as [13]:

$$\begin{aligned}\Phi_{ij} = &-(C_1\epsilon + C_1^* P_k)b_{ij} + C_2\epsilon\left(b_{ik}b_{kj} - \frac{1}{3}b_{kl}b_{kl}\delta_{ij}\right)\\ &+ \left(C_3 - C_3^* II_b^{\frac{1}{2}}\right)kS_{ij} + C_4 k\left(b_{ik}S_{jk} + b_{jk}S_{ik} - \frac{2}{3}b_{kl}S_{kl}\delta_{ij}\right)\\ &+ C_5 k(b_{ik}W_{jk} + b_{jk}W_{ik})\end{aligned} \tag{11}$$

where $S_{ij}\left(=\frac{1}{2}\left(\frac{\partial U_i}{\partial x_j}+\frac{\partial U_j}{\partial x_i}\right)\right)$ is the mean rate of strain, $W_{ij}\left(=\frac{1}{2}\left(\frac{\partial U_i}{\partial x_j}-\frac{\partial U_j}{\partial x_i}\right)\right)$ is the mean vorticity tensor, $b_{ij}\left(=\overline{u_i u_j}/\overline{u_q u_q} - \frac{1}{3}\delta_{ij}\right)$ is the turbulence anisotropy and $II_b\left(=b_{ij}b_{ij}\right)$ is the second invariant of anisotropy. Alternative proposals for modeling this term have been reported, differing only in the relative weighting assigned to the various terms in Eq. (11).

Table 1 Coefficients for the alternative pressure-strain models

Model	C_1	C_1^*	C_2	C_3	C_3^*	C_4	C_5	$C_{\epsilon 1}$	$C_{\epsilon 2}$	C_ϵ
DY	4.0	3.0	0	0.8	2.0	0.6	0	1.45	1.9	0.18
SSG	3.4	1.8	4.2	0.8	1.3	1.25	0.4	1.44	1.83	0.18
GL	3.6	0	0	0.8	0	1.2	1.2	1.44	1.83	0.16

Since the objective of this paper is determine whether a Reynolds-stress transport closure can accurately predict this flow, computations were performed with three of these proposals in order to determine their relative merits. The first of these is due to Gibson and Launder [14] (hereafter referred to as GL). This is arguably the best known and most widely used pressure-strain model and one which differs from the other two considered here in that it requires the specification of a function to represent the effects of a solid wall in damping the fluctuating pressure field in its vicinity. In flows over complex geometries, ambiguity arises in the way in which this function should be specified, though this would not be the case here since only one wall is present, and the flow is predominantly parallel to it. The remaining two proposals do not employ a wall-damping function. They are the proposal by Speziale et al. [15] (hereafter SSG) which contains a contribution term which is quadratic in the Reynolds stresses, and that of Dafalias and Younis [16] (hereafter DY) which is linear in these quantities and which is consistent with the requirement that the model should not depend on vorticity. The coefficients appropriate to these proposals are presented in Table 1.

The final approximation needed to close Eq. (9) relates to the term representing dissipation by viscous action. At high values of the turbulence Reynolds number, the dissipative motions are assumed to be isotropic and the dissipation rate (ϵ) is then obtained from Eq. (7).

2.3 The models for $\overline{u_i\theta}$

In the scalar-flux transport modeling approach, the mass fluxes are obtained from the solution of the transport equation:

$$U_k \frac{\partial(\overline{u_i\theta})}{\partial x_k} = \frac{\partial}{\partial x_k}\left(\frac{\nu}{Sc}\frac{\partial \overline{u_i\theta}}{\partial x_k} + C_\theta \frac{k}{\epsilon}\overline{u_k u_l}\frac{\partial \overline{u_i\theta}}{\partial x_l}\right) + P_{i\theta,1} + P_{i\theta,2} + \pi_{i\theta} \tag{12}$$

In the above, diffusion of $\overline{u_i\theta}$ by turbulent fluctuations has been modeled via gradient-transport assumptions with $C_\theta = 0.15$ Malin and Younis [17]. The rate of dissipation by viscous action vanishes at high turbulence Reynolds numbers and is dropped. The production terms are exact and are given by:

$$P_{i\theta,1} \equiv -\overline{u_k u_i}\frac{\partial \Theta}{\partial x_k} \tag{13}$$

$$P_{i\theta,2} \equiv -\overline{u_k\theta}\frac{\partial U_i}{\partial x_k} \tag{14}$$

The fluctuating pressure–scalar–gradient correlation term ($\pi_{i\theta}$), may be viewed as the counterpart of the pressure–strain term in the $\overline{u_i u_j}$ transport equation and is expected to play an equally role in accounting for the effects of interactions on the mass transport across the wall jet. Its role is generally to reduce $\overline{u_i\theta}$. This term is usually modeled as the sum of three elements:

$$\pi_{i\theta} = \pi_{i\theta,1} + \pi_{i\theta,2} + \pi_{i\theta,w} \tag{15}$$

the separate contributions arising respectively from purely turbulence interactions, interactions between the mean strain and fluctuating quantities and corrections to allow for wall damping. Following Monin [18], and Gibson and Launder [14], these contributions are modeled follows:

$$\pi_{i\theta,1} = -C_{1\theta}\frac{\epsilon}{k}\overline{u_i\theta} \tag{16}$$

$$\pi_{i\theta,2} = -C_{2\theta}P_{i\theta,2} \tag{17}$$

$$\pi_{i\theta,w} = -C_{\theta,w}\frac{\epsilon}{k}\overline{u_i\theta}n_i n_k \mathbf{f} \tag{18}$$

where n_k is the wall-normal unit vector, and f is a wall-proximity function defined as in the original reference. The coefficients of these models, which were determined by reference to measurements of streamwise and cross-stream flux components in homogeneous shear flows Malin and Younis [17], are assigned the values: $(C_{1\theta}, C_{2\theta}, C_{\theta,w}) = (2.85, 0.55, 1.2)$.

While the effects of mean velocity gradients appear explicitly in the exact equation for the turbulent scalar fluxes Eq. (14), these effects are entirely absent from Fick's law which makes the mass fluxes proportional to the gradients of concentration:

$$-\overline{u_i\theta} = \Gamma_t\frac{\partial\Theta}{\partial x_i} \tag{19}$$

The eddy diffusivity Γ_t is related to the eddy viscosity via a relation of the form

$$\Gamma_t = \frac{\nu_t}{Sc_t}\frac{k^2}{\epsilon} \tag{20}$$

where Sc_t is the turbulent Schmidt number.

Several proposals have been made to include an explicit dependence on the gradients of mean velocity in the model for turbulent scalar fluxes (e.g. Yoshizawa [19], Rubinstein and Barton [20]). The one chosen for this study is the model of Younis et al. [21] which was developed by postulating a functional relationship based on the terms that appear in the exact equation and then using tensor representation theory to derive a model which, after simplification, reads:

$$\begin{aligned}-\overline{u_i\theta} = {} & C_1\frac{k^2}{\epsilon}\frac{\partial\Theta}{\partial x_i} + C_2\frac{k}{\epsilon}\overline{u_iu_j}\frac{\partial\Theta}{\partial x_j} \\ & + C_3\frac{k^3}{\epsilon^2}\frac{\partial U_i}{\partial x_j}\frac{\partial\Theta}{\partial x_j} + C_4\frac{k^2}{\epsilon^2}\left(\overline{u_iu_k}\frac{\partial U_j}{\partial x_k} + \overline{u_ju_k}\frac{\partial U_i}{\partial x_k}\right)\frac{\partial\Theta}{\partial x_j}\end{aligned} \tag{21}$$

Note that Fick's law is represented by the first term in Eq. (21). The model coefficients were assigned the values (C_1, C_2, C_3, C_4) = (-0.045, 0.37, -0.0037, -0.023). These values were deduced by the model's originators by calibrating it against the LES and DNS results of Kaltenbach et al. [22] for scalar diffusion in homogeneous turbulence with uniform shear and constant scalar gradients. While the flows under present consideration are very different from those of [22]—being inhomogeneous and with a shear rate that changes sign with distance from the wall—no changes are made to these values on the basis that a properly-formulated model, once calibrated in simple flows should be expected to apply in the more complex flows under present consideration. In what follows, this

model's ability to predict the rate of mass transfer across the interface between the wall and free layers will be assessed.

2.4 The wall functions for smooth and transitionally rough surfaces

When utilizing turbulence closures that are valid only at high turbulence Reynolds numbers, 'wall functions' are needed to bridge the near-wall regions where the turbulence Reynolds number are low and where viscous effects dominate. These functions are based on experimental correlations which, for the case of velocity, are provided by the assumption that the universal logarithmic law of the wall is valid:

$$\frac{U}{u_\tau} = \frac{1}{\kappa}\log y^+ + B \tag{22}$$

where $\kappa = 0.41$ is the von Kármán's constant and $B = 5.0$.

Findings from several experiments on wall jets confirm the applicability of this law for the case where the jet develops over a smooth surface [23, 24]. For the case of a rough surface, Nikuradse [25] classified roughness based on sand grain roughness Reynolds number, defined as $k_s^+ = k_s u_\tau / \nu$. A flow is considered smooth if $k_s^+ \leq 5$, transitionally rough when $5 < k_s^+ < 70$ and rough for $k_s^+ \geq 70$. For the case of transitional roughness that is of interest here, Brzek et al. [26] proposed a power-law relationship that takes the form:

$$\frac{U_m}{u_\tau} = 2\left[\frac{\tilde{C}_o}{\tilde{C}_i}\right]^2 \left(y^+_{\delta,1/2}\right)^{-2\tilde{\gamma}} \tag{23}$$

with the coefficients defined as

$$\tilde{C}_o = C_o(1 + C_{ok}) \tag{24}$$

$$\tilde{C}_i = C_i/(1 + C_{ik}) \tag{25}$$

$$\tilde{\gamma} = \gamma + \gamma_k \tag{26}$$

and

$$C_{ok} = 0.00576\left(k_s^+\right)^{0.517} \tag{27}$$

$$C_{ik} = 0.03551\left(k_s^+\right)^{0.88647} \tag{28}$$

$$\gamma_k = 0.0065\left(k_s^+\right)^{0.60126} \tag{29}$$

This is supplemented by the coefficients given in the proposal of George and Castillo [27]:

$$\frac{C_o}{C_i} = \frac{C_{0\infty}}{C_{i\infty}} \exp\left[\frac{(1+\alpha)A}{\Psi^\alpha}\right] \tag{30}$$

$$\gamma = \gamma_\infty + \frac{\alpha A}{\Psi^{1+\alpha}} \tag{31}$$

where $\Psi = \ln D y^+_{\delta,1/2}$ and the dimensionless half width of the wall jet is defined as $y^+_{\delta,1/2} = y_{\delta,1/2} u_\tau / \nu$. The coefficients used are assigned the values proposed by Rostamy et al. [28] (Table 2).

Table 2 Coefficients for transitionally rough surface wall function, [28]

α	A	γ_∞	D	$C_{0\infty}/C_{i\infty}$
0.46	2.9	0.0362	1.0	0.02385

3 Solution of equations

The equations of Sect. 2 were solved simultaneously by means of the EXPRESS code [29]. This is a finite-volume marching integration method which utilizes transformed coordinates that allow for the computational grid to expand to match the actual width of the wall jet. This is done to ensure that all the computational nodes used remain within the shear layer. Second-order accurate discretisation is employed for both streamwise and cross-stream directions using weighted average approximation for the former and central differencing for the latter. Typically, the simulations were carried out with 60 nodes that were unevenly distributed in the cross-stream direction. Virtually identical results were obtained on grids utilizing 30 and 90 nodes. The solution was started from uniform velocity and concentration profiles and was advanced step by step in the direction of flow. The size of the forward step was limited to 1 % of the local width of the shear layer. At each streamwise location, iterations were performed until the absolute sum of the residuals for all the dependent variables fell to below 10^{-3}. Uniform distributions at inlet were also assumed for the turbulence variables. For the cases of the equilibrium wall jets, the computations were continued until the appropriately non-dimensionalized flow variables ceased to change. The streamwise pressure gradient was deduced from the reduced form of streamwise momentum equation applied in the outer, potential-flow region. The remaining boundary conditions were as follows: at the free stream, the cross-stream gradients of all dependent variables were set equal to zero. At the wall, the fluxes of momentum were deduced either from the universal logarithmic law of the wall (Eq. 22) or from the correlation for transitional roughness (Eq. 23).

4 Results and discussion

4.1 Smooth wall

The first flow considered is that of a wall jet developing over a smooth wall. The experimental data are those of Eriksson et al. [24] who used Laser Doppler Anemometry (LDA) to measure the development of a wall jet, in water, in stagnant surroundings. The Reynolds number (based on exit slot height and velocity) was 9600. The slot width was sufficiently wide for the jet to be essentially two-dimensional. The relative turbulence intensity at exit from the slot was below 1 %.

Figure 2 presents the predicted and measured evolution of mean streamwise velocity with downstream distance from the slot. The velocity is non-dimensionalised by the local maximum value and the cross-stream distance by the jet's half width. In the initial stage of development, at $x/b = 20$, the differential turbulence models appear to slightly overestimate the distance from the wall where the maximum velocity occurs. This is very likely due to a mis-match between the initial conditions in the experiments (not reported but were indicated to involve laminar-turbulent transition; something which is beyond the capabilities of the present models), and those that were assumed in the calculations. To test the

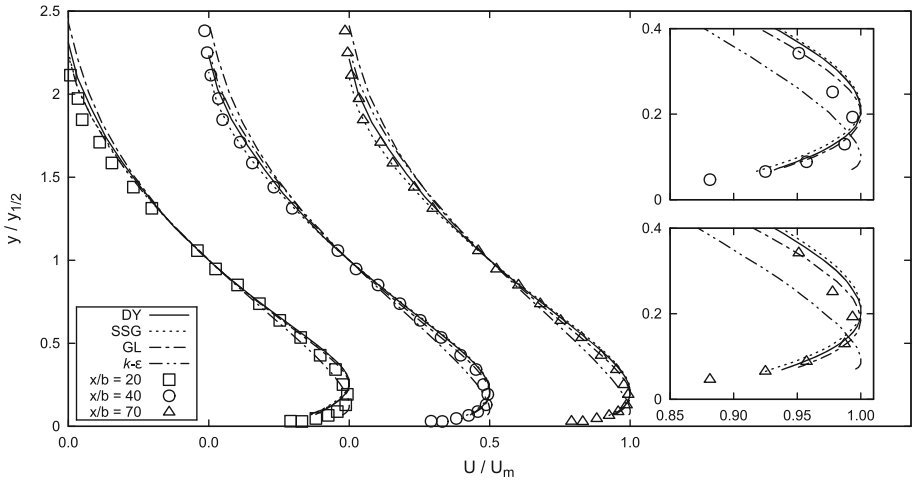

Fig. 2 Predicted and measured streamwise mean velocity. Data of [24]

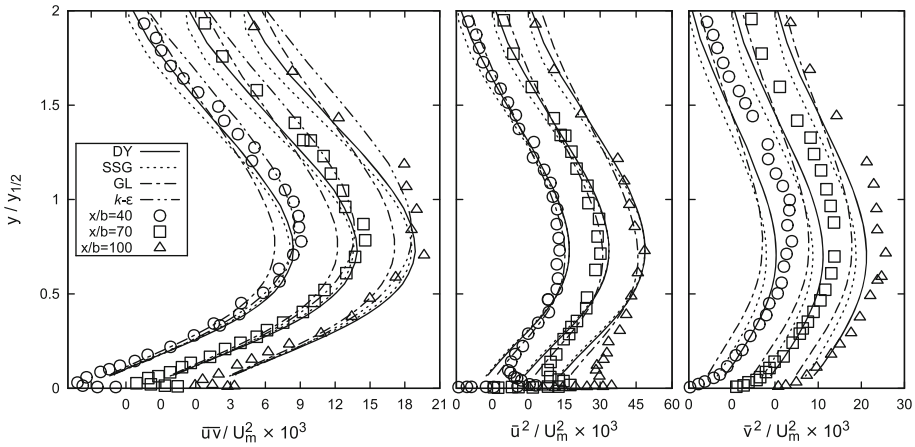

Fig. 3 Predicted and measured streamwise variation of Reynolds stresses. Data of [24]

sensitivity of the computations to the assumed initial level of turbulence intensity, calculation were performed with relative intensity levels of 1, 5 and 10 % with no significant differences observed. The influence of the initial conditions recedes with increasing distance from the slot where the jet eventually transitions to a fully-turbulent state. There, the differential models are in close agreement with the measurements. In contrast, the k-ϵ model does not accurately predict the location of the velocity maximum—a result which, as will be seen later, arises from the incorrect prediction of the turbulent shear stress there (Fig. 3).

In Fig. 3, the predicted and measured cross-stream profiles of the turbulent stresses are compared. The shear stress $\overline{uv}$ enters, via its spatial gradients, into the balance of streamwise momentum. The maximum value of this stress is therefore very influential in determining the rate of momentum transfer across the interface and, consequently, in the shape of streamwise velocity profile especially near the maximum. Here again it can be

seen that the differential models yield essentially similar results that correspond fairly closely to the experimental data. Close to the wall, the models results are indistinguishable but in the mid-region of the free shear layer (f $y/y_{1/2} = 1$), the GL model underestimates the measured values which suggests that the influence of the wall-damping functions that are unique to that model extend somewhat too far from the wall. The maximum shear stress is underestimated by the k-ϵ model leading to the observed large differences in the mean-velocity profiles. The profiles of the normal-stress component $\overline{u^2}$ show a maximum near the wall, followed by a steep drop to a minima in the where the velocity gradient and the shear stress (and consequently its rate of production) are zero. The normal stress remains finite being maintained by diffusion. Beyond this point, $\overline{u^2}$ recovers and reaches a maximum at around the mid-point of the free layer where the shear stress and the mean velocity gradient are near their maxima. The profile of $\overline{v^2}$ is less eventful in that it shows a monotonic rise away from the wall until reaching a maxima at mid-layer before falling off to zero in the free stream. While there is no direct energy generation into this component, it is maintained by energy redistribution from $\overline{u^2}$ via the pressure-strain terms. The DY model appears to perform the best in capturing this redistribution.

A wall jet attains the self-preserving condition when its half width grows linearly with downstream distance and the spreading rate attains a constant value. The predicted and measured growth of the jet's half width is presented in Fig. 4. A mean spreading rate in the region between $x/b = 20$ and $x/b = 200$ was calculated for comparison with the experimental data. Eriksson gives a spreading rate of 0.078. In their extensive survey, Launder and Rodi [30] quoted a spreading rate of 0.073 ± 0.002 for a plane wall jet in stagnant surroundings. George and Castello [31] demonstrated that the spreading rate is not necessarily strictly independent of x but that there's a dependence on Reynolds number as well. In this study, the calculated spreading rates were 0.0791 for the DY model, 0.0769 for SSG, and 0.0726 for the GL model. The k-ϵ model result was 0.0805 which is on par with the GL model in terms of relative difference with the measurements.

The predicted variation of the skin-friction coefficient $C_f\,(= 2(U_\tau/U_m)^2)$ with $Re_m(= U_m b/v)$ is shown in Fig. (5). These results were obtained from a single run. Also plotted there are measurements by Abrahamsson et al. [32] and the correlations of Bradshaw and Gee [33] $\left(C_f = 0.0315 Re_m^{-0.182}\right)$. There is little that distinguishes the differential stress models results from each other while the k-ϵ model results are significantly lower. Since the wall shear stress is among the principal parameters that determine the rate of bed-load

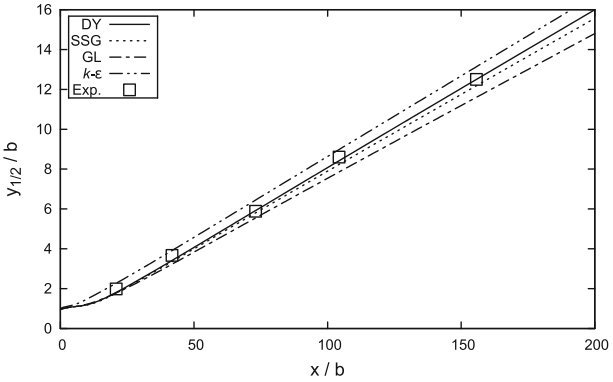

Fig. 4 Variation of jet half-width with distance. Data of [24]

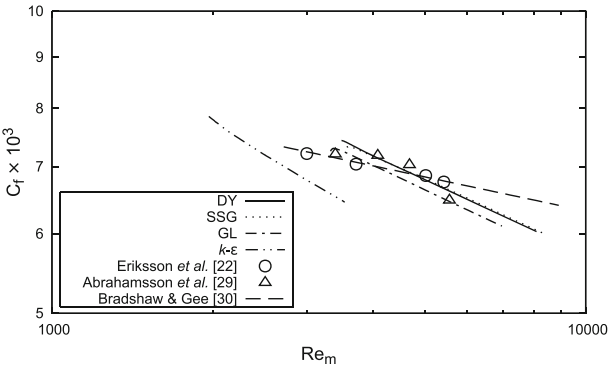

Fig. 5 Variation of C_f with Re_m for wall jet on plane smooth surface

transport, it is to be expected that the extent of scour in an erodible boundary would be significantly underpredicted by this model.

4.2 Smooth wall with mass transfer

Attention is now turned to the case of mass transport in a wall jet, specifically to determination of the mass-transfer rates at the wall, and the resulting cross-stream profiles of concentration. The predictions are compared with the measurements obtained by Mabuchi and Kumada [34] in a jet developing over a plane napthalene covered surface. The napthalene method is an excellent source for experimental data on mass transport since the results are well reproducible and the accuracy is high with the experimental uncertainty estimated to be $\approx 7\,\%$ for $\pm 2\sigma$ Goldstein and Cho [35]. The jet was issued from a rectangular slot with $Re_0 = 17{,}200$ into stagnant surroundings. Using typical values for air at ambient temperatures and the mean nozzle exit velocity of $U_0 = 51.6$ m s^{-1} a slot height of $b = 5.27$ mm was calculated. A trip wire was placed at the nozzle exit to accelerate the transition to turbulent conditions. The measured relative turbulence intensity at exit was ≈ 0.6 %. The Sherwood number (Sh), which is the dimensionless gradient of concentration at the wall and which physically represents the ratio of convective to diffusive mass transfer, was obtained in the experiments by measuring the sublimation of napthalene. The laminar Schmidt number at ambient temperature $T = 295.25$ K was obtained from the correlation $Sc_l = 2.28\,(T/298.16)^{-0.1526}$ [35]. The turbulent Schmidt number was taken as $Sc_t = 0.9$.

The predicted and measured profiles of mean velocity are compared in Fig. 6a. It can again be seen that the differential stress models yield predictions that are in good agreement with the experimental data. In contrast, and as before, the k-ϵ model result is significantly at variance with the data, especially in the near wall area. The cross-stream profiles of mean concentration are presented in Fig. 6. The profiles have been non-dimensionalized with the maximum value which is obtained at the wall. For clarity, only the results obtained with the DY model are presented—these are representative of the other models' predictions. No experimental data are available for comparisons. The most notable observation is the close correspondence between the predictions of the complete mass-flux transport closure, and the algebraic model of [21] which allows for the turbulent mass fluxes to depend on the gradients of both mean concentration and mean velocity. The results obtained with Fick's law are distinctly different from the other models', in both the near-wall and the free shear flow regions.

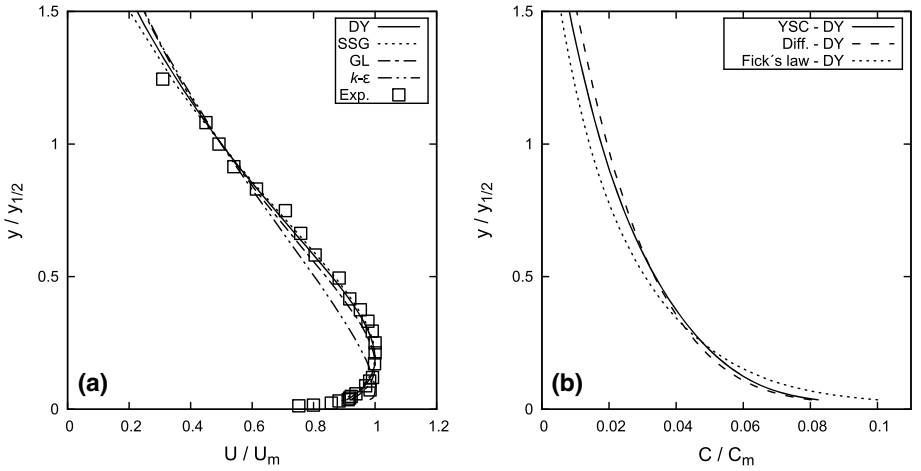

Fig. 6 **a** Predicted and measured velocity distribution at $x/b = 25$. Data of [34]. **b** predicted profiles of mean concentration

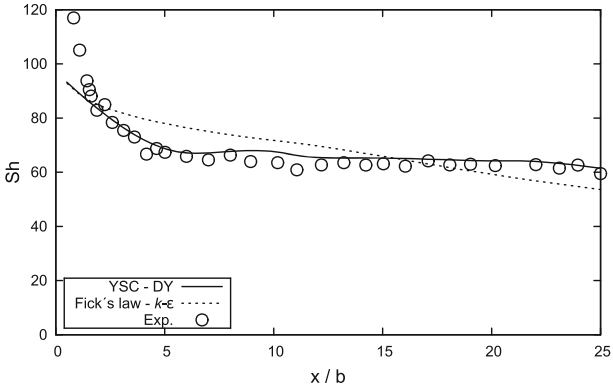

Fig. 7 Near-field variation of Sherwood number with streamwise distance. Data of [34]

The predicted and measured variation of Sherwood number at the surface with streamwise distance from the virtual origin is presented in Fig. 7 for the near-field zone, and in Fig. 8 for the far field. Plotted there are the results obtained with the three models for the turbulent mass fluxes. The flow field predictions were obtained using the DY model. The results show that the algebraic YSC model and the differential mass-flux model yield identical results that accord very closely with the measurements. The exception being close to the nozzle exit where the initial conditions that prevailed in the experiments are not well specified. In contrast, Fick's law, in combination with the k-ϵ model, yields results that are significantly at variance with the measurements.

4.3 Transitionally rough wall

Recent measurements of a wall jet developing over a transitionally rough surface were reported by Rostamy et al. [28]. The measurements were obtained in a water flume using

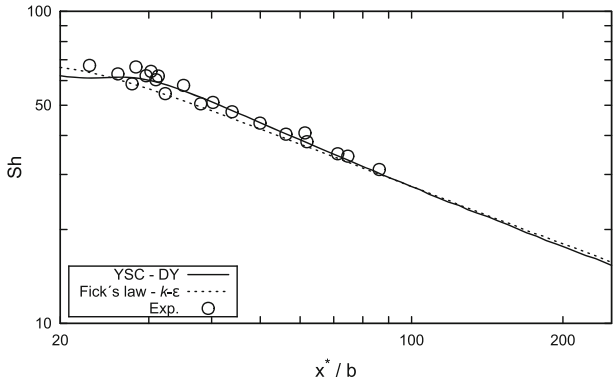

Fig. 8 Far-field variation of Sherwood number with distance. Data of [34]

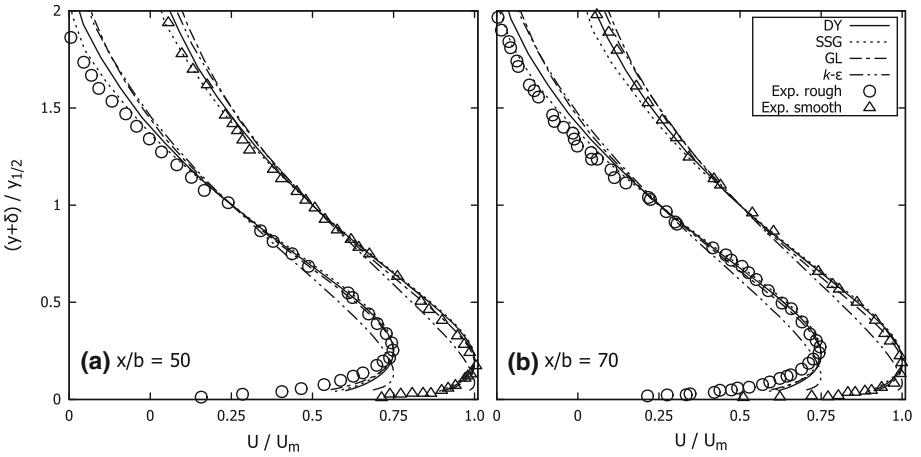

Fig. 9 Velocity profiles for transitionally rough and smooth surfaces at: **a** $x/b = 50$, **b** $x/b = 70$. Data of [28]

LDA. The Reynolds number was $Re_0 = 7500$, with a slot height of $b = 6$ mm and a mean exit velocity $U_0 = 1.21$ m s^{-1}. The relative turbulence intensity at the nozzle exit was less than 1 %. To generate roughness, a grit sheet with a nominal grain size of $k_g = 0.53$ mm was positioned at $x = 10b$. The equivalent sand grain roughness size was estimated to be $k_s \approx 1.1$ mm.

The predicted and measured cross-stream profiles of mean velocity for flow over the transitionally rough surface are compared in Fig. 9. Measurements obtained in the same study for a flow over a smooth surface are included for comparison. Profiles are presented for two downstream locations. The k-ϵ model results are clearly in error at both locations. The transitionally rough profiles for the differential stress models all appear to overestimate the measurements near the wall. The SSG model produces markedly better agreement with the measurements in the region adjacent to the free stream. This is due to the inclusion in this model of terms that are quadratic in the Reynolds stresses (the C_2 term in Eq. 11). The contribution of these terms to the overall level of the pressure-strain correlations has been shown to become influential in the development of free shear flows

[36] and hence the observed improvement in its prediction of the outer regions of the wall jet.

For a self-similar mean velocity profile the momentum field can be characterized by the following relation [37]:

$$\int_0^\infty U^2 dy = \lambda U_m^2 y_{1/2} \tag{32}$$

where

$$\lambda = \int_0^\infty \left[\frac{U}{U_m}\right]^2 d\left(\frac{y}{y_{1/2}}\right) \tag{33}$$

The values obtained with the different turbulence models are compared with the experimental data by Rostamy and Wygnanski in Table 3. The DY and SSG models results are closest to the measured values, while the GL model yields a lower value. The k-ϵ model results are significantly lower still. A comparison for the spreading rate is also given in Table 3. According to Rostamy there is almost no change in the spreading rate due to transitional roughness. This is borne out in the Reynolds-stress models results (Fig. 10).

The variation of friction coefficient with Reynolds number is shown in Fig. 10. The present predictions are compared with the measurements of Tachie et al. [23] and Eriksson et al. [24]. For the smooth wall case, the DY and SSG models yield almost

Table 3 Predicted and measured momentum field characterization and spreading rates for smooth and transitionally rough surfaces

	λ		$dy_{1/2}/dx \cdot 10^{-2}$	
	Smooth	Rough	Smooth	Rough
Wygnanski et al. [37]	0.74	–	–	–
Rostamy et al. [28]	0.745	0.731	7.91	8.06
DY	0.739	0.741	8.98	9.00
SSG	0.740	0.742	8.71	8.75
GL	0.731	0.734	8.14	8.10
k-ϵ	0.699	0.705	9.17	9.12

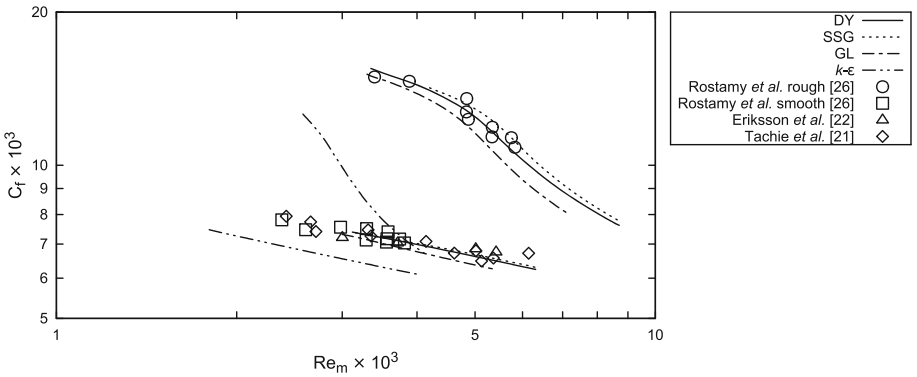

Fig. 10 Skin-friction coefficient in transitionally rough wall jet

indistinguishable results in contrast with the k-ϵ model which obtains significantly lower values. For the rough wall case, the DY and SSG models again yield a close match to the data while the k-ϵ model significantly underestimates the velocity in the near-wall region.

5 Concluding remarks

The paper puts on record the capabilities and limitations of a number of turbulence closures in predicting the transport of mass and momentum in wall jets developing over smooth and transitionally-rough surfaces. The turbulence closures consisted of the widely-used k-ϵ model, and the more advanced closures that require the solution of modeled differential transport equation for each component of the Reynolds-stresses and the mass fluxes. Also considered is an algebraic model for the turbulent mass fluxes that allows for the dependence of these fluxes on the gradients of both the mean concentration and the velocity. Alternative proposals for modeling the unknown fluctuating pressure strain correlations were assessed with reference to detailed measurements of turbulent wall jets developing over smooth surfaces. It was found that the three proposals examined yielded essentially similar results with the DY model offering best overall performance (Table 4; Fig. 11). The results also suggest that the use of the model of the GL model is not recommended for these flows as it involves the use of a wall-damping function whose influence extends well into the outer region. While all the differential models succeeded in reproducing the measured variation of wall shear stress with Reynolds number, the k-ϵ closure failed badly in this respect producing results that seriously underestimate this parameter. Since the wall shear stress is the driving parameter in nearly all models for bedload sediment transport, the present results would suggest that the use of this model will produce erroneous results leading to, for example, underestimating the extent of bed scour. Concerning the rate of mass transfer from the wall, a process that plays an important part in determining the occurrence and extent of sediment re-suspension, the use of the k-ϵ model together with Fick's law again produces results that are at variance with the measurements. In contrast, both the differential and the extended models for the turbulent mass fluxes provide an accurate prediction of the mass transfer rate yielding essentially indistinguishable results. This argues in favor of using the simpler, extended algebraic model for predicting sediment transport post re-suspension.

Acknowledgments M. Zumdick gratefully acknowledges the financial support provided by the Hermann-Reissner-Stiftung to support his stay at the University of California, Davis.

Appendix: Numerical accuracy

Grid-independence tests were performed with the number of cross-stream nodes varied by a factor of 3 viz. 30, 60 and 90. The differences between the results obtained with the finest and the coarsest grids was of the order of 1 % (e.g. the jet's spreading rate, a sensitive parameter whose value is detemined by the details of the turbulence field, was predicted with the 30 nodes simulations to be 0.079 and with the 90 nodes simulations to be 0.078). The reasons for such small dependence of the computed results on the grid arise from the fact that the flow is uni-directional and is thus largely free of the interpolation errors that arise when the flow streamlines are not aligned with the grid lines. Indeed the computational grid is

designed so as to adapt to the physical extent of the flow and in this way remain aligned with the streamlines, and with all the cross-stream nodes always located within the flow.

Quantification of the degree of correspondence between the predictions and the measurements of Eriksson et al. [24] is presented in Table 4 for the maximum values of the Reynolds stresses at three streamwise locations, and in Fig. 11 for the cross-stream profiles of streamwise velocity. Undoubtly some of the observed differences arise from shortcomings in the models but it should also be noted that the experimental results themselves are subject to uncertainties. In this regard, it is interesting to note that all the models yield differences that are positive in sign which may suggest that the measurements underestimate the actual values to some extent. Figure 11 also shows that the percentage differences decrease markedly with distance from the nozzle exit. This is to be expected considering that the starting profiles for the computations had to be assumed due to the absence of measurements there.

See Table 4 and Fig. 11.

Table 4 Percentage difference beween predicted and measured maximum Reynolds stresses

	$\overline{uv}/U_m^2$			u^2/U_m^2			v^2/U_m^2		
$x/b =$	40	70		40	70	100	40	70	100
Exp.	0.0151	0.0156	0.0157	0.0431	0.0451	0.0485	0.0234	0.0238	0.0257
DY (%)	19.1	7.6	4.8	7.8	4.4	0.4	29.9	15.0	17.7
SSG (%)	22.4	9.6	6.7	8.5	4.4	0.4	38.0	24.2	26.7
GL (%)	31.0	17.9	15.7	8.8	0.4	5.0	45.3	28.0	30.6
k-ϵ (%)	6.5	7.0	6.1	–	–	–	–	–	–

Data of Eriksson et al. [24]

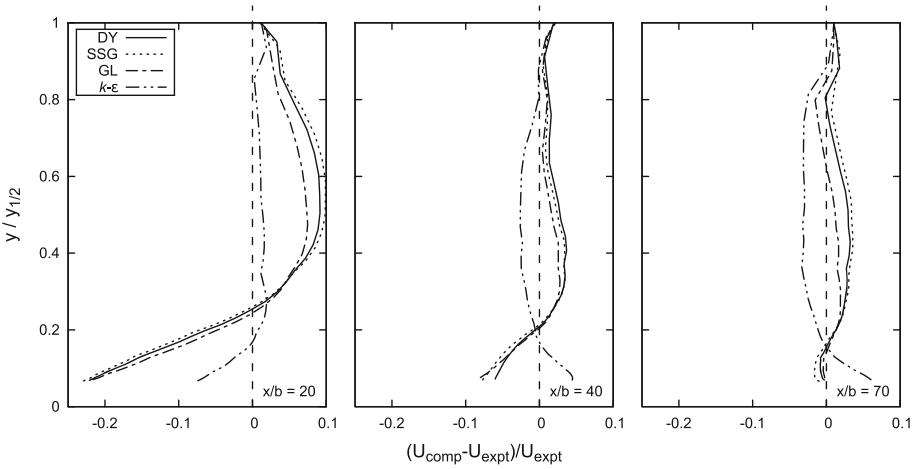

Fig. 11 Cross-stream variation of relative differences beween predicted and measured mean velocity. Data of Eriksson et al. [24]

References

1. Rastello M, Hopfinger EJ (2004) Sediment-entraining suspension clouds: a model of powder-snow avalanches. J Fluid Mech 509:181–206. doi:10.1017/S0022112004009322
2. Etienne J, Rastello M, Hopfinger EJ (2006) Modelling and simulation of powder-snow avalanches. C R Mécanique 334:545–554. doi:10.1016/j.crme.2006.07.010
3. Kneller B, Buckee C (2000) The structure and fluid mechanics of turbidity currents: a review of some recent studies and their geological implications. Sedimentology 47:62–94
4. Gray TE, Alexander J, Leeder MR (2005) Quantifying velocity and turbulence structure in depositing sustained turbidity currents across breaks in slope. Sedimentology 52:467–488
5. Mazurek KA, Rajaratnam N, Sego DC (2003) Scour of a cohesive soil by submerged plane turbulent wall jets. J Hydraul Res 41:195–206
6. Rajaratnam N (1981) Erosion by plane turbulent jets. J Hydraul Res 19:339–358
7. Hogg AJ, Huppert HE, Dade WB (1997) Erosion by planar turbulent wall jets. J Fluid Mech 338:317–340. doi:10.1017/S0022112097005077
8. Barenblatt GI, Chorin AJ, Prostokishin VM (2005) The turbulent wall jet: a triple-layered structure and incomplete similarity. Proc Nat Acad Sci 102:8850–8853. doi:10.1073/pnas.0503186102
9. Gibson MM, Younis BA (1982) Modelling the curved turbulent wall jet. AIAA J 20:1707–1772
10. Albayrak I, Hopfinger EJ, Lemmin U (2008) Near-field flow structure of a confined wall jet on flat and concave rough walls. J Fluid Mech 606:27–49
11. Irwin HPAH (1973) Measurements in a self-preserving plane wall jet in a positive pressure gradient. J Fluid Mech 61:33–63. doi:10.1017/S0022112073000558
12. Daly BJ, Harlow FH (1970) Transport equations in turbulence. Phys Fluids 13:2634–2649. doi:10.1063/1.1692845
13. Younis BA, Speziale CG, Berger S (1998) Accounting for effects of a system rotation on the pressure-strain correlation. AIAA J 36:1746–1748
14. Gibson MM, Launder BE (1978) Ground effects on pressure fluctuations in the atmospheric boundary layer. J Fluid Mech 86:491–511. doi:10.1017/S0022112078001251
15. Speziale CG, Sarkar S, Gatski TB (1991) Modeling the pressure-strain correlation of turbulence: an invariant dynamical systems approach. J Fluid Mech 227:245–272. doi:10.1017/S0022112091000101
16. Dafalias YF, Younis BA (2009) Objective model for the fluctuating pressure-strain-rate correlations. J Eng Mech 135:1006–1014. doi:10.1061/(ASCE)EM.1943-7889.0000014
17. Malin MR, Younis BA (1990) Calculation of turbulent bouyant plumes with a Reynolds stress and heat flux transport closure. Int J Heat Mass Trans 33:2247–2264. doi:10.1016/0017-9310(90)90124-D
18. Monin AS (1965) On the symmetry properties of turbulence in the surface layer of air. Izvestya Atmos Ocean Phys 1:45–54
19. Yoshizawa A (1988) Statistical modelling of passive-scalar diffusion in turbulent shear flows. J Fluid Mech 195:541–555. doi:10.1017/S0022112088002514
20. Rubinstein R, Barton JM (1991) Renormalization group analysis of anisotropic diffusion in turbulent shear flows. Phys Fluids 3:415–421. doi:10.1063/1.858097
21. Younis BA, Speziale CG, Clark TT (2005) A rational model for the turbulent scalar fluxes. Proc R Soc A 461:575–594. doi:10.1098/rspa.2004.1380
22. Kaltenbach HJ, Gerz T, Schumann U (1994) Large-eddy simulation of homogeneous turbulence and diffusion in stably stratified shear flow. J Fluid Mech 280:1–40. doi:10.1017/S0022112094002831
23. Tachie MF, Balachandar R, Bergstrom DJ (2002) Scaling the inner region of turbulent plane wall jets. Exp Fluids 33:351–354. doi:10.1007/s00348-002-0451-6
24. Eriksson JG, Karlsson RI, Persson J (1998) An experimental study of a two-dimensional plane turbulent wall jet. Exp Fluids 25:50–60. doi:10.1007/s003480050207
25. Nikuradse J (1933) Strömungsgesetze in rauhen Rohren. VDI-Forschungsheft 361
26. Brzek B, Bailon-Cuba J, Leonardi S, Castillo L (2009) Theoretical evaluation of the Reynolds shear stress and flow parameters in transitionally rough turbulent boundary layers. J Turbul 10:1–28. doi:10.1080/14685240802524392
27. George WK, Castillo L (2009) Zero-pressure-gradient turbulent boundary layer. Appl Mech Rev 50:689–729. doi:10.1115/1.3101858
28. Rostamy N, Bergstrom DJ, Sumner D, Bugg JD (2011) An experimental study of a turbulent wall jet on smooth and transitionally rough surfaces. J Fluids Eng 133:111207. doi:10.1115/1.4005218
29. Younis BA (1996) EXPRESS: accelerated parabolic Reynolds stress solver. Hydraulics section report HDBAY1, City University, London
30. Launder BE, Rodi W (1981) The turbulent wall jet. Prog Aero Sci 19:81–128

31. George WK, Abrahamsson H, Eriksson J, Karlsson RI, Lofdahl L, Wosnik M (2000) A similarity theory for the turbulent plane wall jet without external stream. J Fluid Mech 425:367–411. doi:10.1017/S002211200000224X
32. Abrahamsson H, Johansson AV, Löfdahl L (1994) A turbulent plane 2-dimensional wall jet in a quiescent surrounding. Eur J Mech B Fluids 13:533–556
33. Bradshaw P, Gee MT (1960) Turbulent wall jets with and without an external stream. Aero R Council R&M 3252
34. Mabuchi I, Kumada M (1972) Studies on heat transfer to turbulent jets with adjacent boundaries. I. Flow development and mass transfer in plane turbulent wall jet. Bull JSME 15:1236–1245
35. Goldstein RJ, Cho HH (1995) A review of mass transfer measurements using naphthalene sublimation. Exp Therm Fluid Sci 10:416–434. doi:10.1016/0894-1777(94)00071-F
36. Younis BA, Gatski T, Speziale CG (1996) Assessment of the SSG pressure-strain model in free turbulent jets with and without swirl. J Fluid Eng 118:800–809
37. Wygnanski I, Katz Y, Horev E (1992) On the applicability of various scaling laws to the turbulent wall jet. J Fluid Mech 234:669–690. doi:10.1017/S002211209200096X